# Comparison of LSST and DECam Wavefront Recovery Algorithms

Bo Xin[a], Aaron Roodman[b], George Angeli[a], Chuck Claver[a], and Sandrine Thomas[a]

[a]Large Synoptic Survey Telescope, Tucson AZ, USA
[b]SLAC National Accelerator Laboratory, Stanford University, Menlo Park CA, USA

## ABSTRACT

We make a detailed quantitative comparison of the wavefront recovery algorithms between those developed for Dark Energy Camera (DECam) and the Large Synoptic Survey Telescope (LSST). Samples used in this study include images of out of focus stars collected by the DECam at the Blanco 4-meter telescope and artificial simulated donut images. The data from DECam include wavefront images collected by the wavefront sensors and out-of-focus images where the entire DECam sensor array is used. For simulated images, we have used both the forward Fraunhofer diffraction and a LSST-like ZEMAX optical model where the images are convolved with Kolmogorov atmosphere. All samples are analyzed with the forward wavefront retrieval algorithm developed for DECam and the transport of intensity algorithm for LSST. Good quantitative agreement between results by the two implemented algorithms is observed.

**Keywords:** LSST, DECam, Wavefront Sensors, Curvature Sensors, Donuts

## 1. INTRODUCTION

The Large Synoptic Survey Telescope (LSST) is a new facility now under construction that will survey ∼20000 square degrees of the southern sky through 6 spectral filters (*ugrizy*) multiple times over a 10-year period.[1,2] The optical system is based on a modified Paul-Baker 3-mirror telescope design having an 8.4m primary, 3.4m secondary, and 5.0m tertiary feeding a three-element refractive camera system producing a flat 9.6 square degree field-of-view with an effective clear aperture of ∼6.5m. LSST will use an active optics system (AOS) to maintain alignment and surface figure on its three large mirrors. Corrective actions fed to the LSST AOS are determined from information derived from 4 curvature wavefront sensors located at the 4 corners of the focal plane. Each wavefront sensor is a split detector such that the halves are 2mm on either side of focus.

The LSST wavefront sensing software is described in detail in Ref. 3. It includes extensions to published curvature wavefront sensing algorithms needed to address challenges presented by the LSST, namely the large central obscuration, the fast $f/1.23$ beam, off-axis pupil distortions, and vignetting at the sensor locations. It also takes into account corrections needed for the split sensors and the effects from the angular separation of different stars providing the intra- and extra-focal images. The underlying baseline algorithms are the iterative Fast Fourier Transform (FFT) method by Roddier and Roddier,[4] and the series expansion technique by Gureyev and Nugent.[5] Ref. 3 also describes a set of very extensive tests and validations using simulated images. However, there is no validation using real data or direct comparison to other wavefront sensing algorithms. In this paper, we present a detailed quantitative comparison with the forward modeling algorithm that has been used by Dark Energy Camera (DECam), using both data collected by the DECam and simulated images.

DECam is a 3 square-degree field-of-view imager now in operation on the CTIO Blanco 4-meter telescope.[6] It has eight wavefront sensors placed on the same focal plane as the 62 science sensors, and a hexapod to allow rapid adjustment of the camera's focus and alignment with respect to the primary mirror. The wavefront sensors are divided into four pairs of intra- and extra-focal sensors, located on the edge of the field of view. Each pair consists of two 2k by 2k CCD chips, placed out of focus by ±1.5mm. The wavefront sensing and the AOS on the DECam have been proven to operate successfully, maintaining unsupervised control of the focus and alignment.[7]

Further author information:
Bo Xin: E-mail: bxin@lsst.org, Telephone: 1 520 318 8352

Given the similarity between the LSST and DECam, both being suvery telescopes with large field-of-view, and both employing area wavefront sensors, DECam can serve as a good test ground for the LSST wavefront sensing software.

The DECam wavefront estimation utilizes a forward-modeling non-linear $\chi^2$ fit.[7] The intensity distribution on the image plane is modeled as the Fraunhofer integral, where the inputs are the pupil function and the wavefront at the exit pupil. The pupil function is a fixed property of DECam and accounts for DECam's complicated obscuration geometry. The wavefront is decomposed into a set of Zernike polynomials, where the coefficients are the free parameters in the fit. The atmospheric seeing is accounted for using a convolution of the image model with a Kolmogorov kernel.

For LSST, the degrees of freedom that need to be controlled include those in the two actively supported mirror systems and the positioning of the two hexapods. The number of degrees of freedom is significantly greater than any currently operating telescopes including DECam. This requires the ability to estimate higher-order properties of the aberrated wavefront. The current design is that Zernike coefficients, Z4 – Z22 in Noll/Mahajan's definition,[8,9] will be measured and used by the AOS. For this reason, LSST has chosen to solve the transport-of-intensity equation (TIE) to retrieve the wavefront, rather than a forward-modeling approach. For DECam online operations, Zernike coefficients up to trefoid (Z9, 10) are measured, and only focus (Z4), astigmatism (Z5, 6), and coma (Z7, 8) are used to control the prime-focus camera's five degrees of freedom. Furthermore, the DECam forward-modeling algorithm fixes the spherical aberration (Z11) to a value predicted by the ZEMAX prescription. The Fried parameter of the atmosphere is fixed at $r_0 = 0.125$m.[7] For offline analysis, the forward fit includes Z11 and $r_0$ as free parameters. In the comparison study presented in this paper, the DECam results come in two versions, one with fits to Zernikes up to Z11, the other with additional quadrafoil (Z14, 15). In the rest of this paper, the indexing and normalization of the Zernikes always follow the Noll/Mahajan's definition.

We also need to note that this comparison study is actually a comparison between the LSST implementation of the baseline algorithms with the iterative wavefront compensation and the DECam forward modeling algorithm. In order to make comparison, the LSST software is run in its "paraxial lens" mode, meaning the algorithm's LSST specific extensions as described in Ref. 3 are being bypassed. Because the DECam software only has the standard circular Zernikes implemented, results from LSST used for comparison are also in standard Zernikes. The obscuration ratio of DECam is 34%. This is less of a problem compared to working with LSST-like images, where the obscuration is 61%. Similarly, DECam is a $f/2.9$ system, while LSST is $f/1.23$. DECam is 2.2 degree wide field, LSST is 3.5 degree. Given DECam's proven success, we expect none of these to lead to significant issues to the comparison study.

This paper is organized as follows. In Section 2 we describe the data used in this analysis, including both images taken by DECam and simulated data. Section 3 then outlines the analysis approach. The results are discussed in Section 4. In Section 5 we give a summary and what we conclude from this analysis.

## 2. DATA OVERVIEW

The comparison study is performed by analyzing the same ensembles of donut images using separate code implementing each of the two algorithms. Samples used in this study include images of out of focus stars collected by the DECam at the Blanco 4-meter telescope and artificial simulated donuts. We have looked at three types of data collected by the DECam during 2014 – 2015: (1) Wavefront sensor images taken during engineering runs, when the telescope was doing large slews throughout the night, with open AOS loop, without the look-up-table corrections. We'll later refer to these as the open-loop data. In these data, the wavefront aberrations vary more wildly compared to the normal observing runs. (2) Wavefront sensor images taken during typical DECam observing nights. (3) Science sensor images taken during engineering runs, where the entire camera was moved out of focus. These also do not have the AOS corrections. For the wavefront sensor images, including types (1) and (2) above, the images from adjacent CCDs are from both sides of focus at ±1.5mm. They can therefore directly be used by the LSST software. The out-of-focus science images (type (3)) are also from both sides of focus, at ± 1.5mm and ±3.0mm. These were used by DECam to map out the wavefront across the focal plane. Both softwares use the cut-out images created by the DECam wavefront image pre-processing pipeline. The image stamps are 64 by 64 pixels for ±1.5mm defocused images and 128 by 128 for ±3.0mm

defocused images. The number of DECam exposures that are used in the analysis is 202, 137, and 98 for types (1), (2), and (3), respectively. The number of postage stamps are 58,997, 10,688, and 174,472 for the three types of data, before any selection that will be discussed in the next section.

Tests using simulated images have the advantage of being able to better cover the parameter space. We have used two sets of simulated images. In the first set, the forward-modeling code utilizing the forward Fraunhofer diffraction intergral, which is part of the DECam algorithm, is used to generate the synthetic donut images. The wavelength is 700nm. The second set of test images are generated using a simple ZEMAX paraxial lens model, with $f/1.23$ and central obscuration of 61%. The parameters are the same as the LSST optical system, but the model doesn't have the fast-beam non-linear effects and the off-axis distortions. Geometric Image Analysis is performed at 1mm above and below the focus. Both sets of images are then convolved with Kolmogorv PSF kernels representing the atmospheric seeing. For each Zernike among Z4 – Z15, intra- and extra-focal images are simulated for magnitudes of 0.05, 0.10, 0.25, 0.50, 1.00, 1.50, and 2.00 waves, with wavelength of 770nm.

## 3. ANALYSIS APPROACH

The DECam wavefront sensing algorithm only requires one donut image at a time, in order to fit for the wavefront. For the TIE-based LSST algorithm, both intra- and extra-focal images are required. Ideally, the TIE requires that the intra- and extra-focal images be taken with the same optics state and at the same field position. With the area sensors, these conditions can not be satisfied. We need to minimize the difference between the intra- and extra-focal images, in terms of their field positions and how much the telescope state might have changed between them if they are from separate exposures. Another consideration is that if we match an intra-focal image with good Signal-to-Noise Ratio (SNR) with an extra-focal image with bad SNR, and vice versa, we will not get a good wavefront measurement. Therefore, care needs to be taken when pairing images from different sources.

On the wavefront sensor images from each exposure, we typically have tens of donut images on each of the eight sensors. Because the wavefront varies across the focal plane, we only use images from adjacent CCDs to form the intra- and extra-focal pairs. Saturated images are excluded from further use. DECam chips saturate at around 40,000 counts, except that FS4* (amplifier with column number $IX$ >1024) and FN2 (amplifier with $IX$ <1024) saturate at much lower - around 5000 counts. We then remove the background by means of a least-square fit to the intensity outside of the signal region using a 2D linear model. The signal region is defined as an annulus large enough to cover the aberrated signals. The SNR is then calculated for each donut image based on this fit. To make sure the input images are of good quality, donut images with SNR less than 20 are not used. Next, all the donuts on each wavefront sensor are ranked using SNR from high to low. Intra- and extra-focal pairs are then formed by taking the first image from the intra-focal sensor and the first image from the extra-focal sensor, the second image from the intra-focal sensor and the second image from the extra-focal sensor, and so on, until the list on either sensor is exhausted. As an example, Figure 1 (left) shows one pair of intra- and extra-focal images on the wavefront sensors with the telescope in the open-loop mode. With 15$\mu$m DECam pixels, the donuts are roughly 40 pixels in diameter. The SNR distributions on the pairs of wavefront sensors for the same exposure is shown in Figure 1 (right). The number of image pairs that pass the above selection criteria are 6,284, 1,344, and 29,427 for data types (1), (2), and (3).

After running the LSST wavefront sensing software on each of these image pairs, the recovered wavefronts, in terms of Zernike coefficients, are averaged over the same pair of wavefront sensors. These are then compared to the results from the DECam algorithm. For each pair of images used by the LSST algorithm, there are two sets of Zernike coefficents from the DECam algorithm, each from one image. The Z4 values are approximately $\pm 8.7\lambda$, where the wavelength $\lambda$=700nm. To compare to results from the LSST software, we average each Zernike over the adjacent sensors, to get one set of Zernikes for each sensor pair. Bad fits are excluded by requiring that the RMS of Z5 – Z10 be less than 3$\mu$m and the magnitude of measured Z4 on each individual image be between 5$\mu$m and 15$\mu$m.

For the out-of-focus DECam images, we follow the same procedure as described above for the wavefront images, except the pairing. After ranking the donut images from each sensor based SNR from high to low, the

*The naming of the DECam sensors can be found in, for example, Figure 1 of Ref. 7.

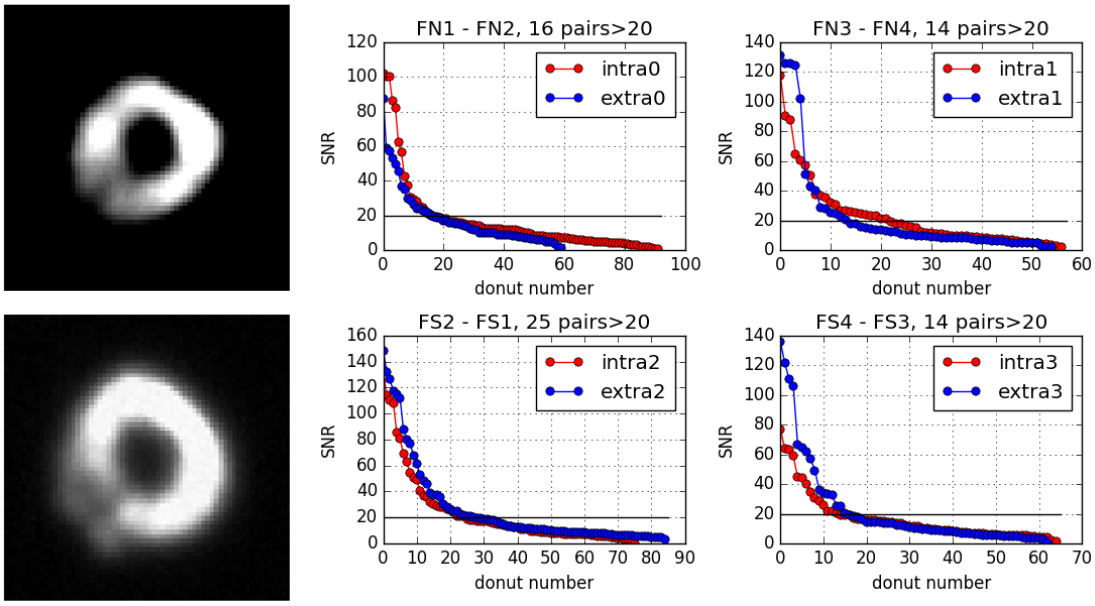


Figure 1. Left: An intra-focal image (top) on wavefront sensor FN1 and an extra-focal image (bottom) on wavefront sensor FN2. Right: SNR distributions on the pairs of wavefront sensors. The plot titles show the sensor names and the number of image pairs where both images have SNR >20. These examples are with the telescope in the open-loop mode.

image pairs are formed by taking one image from an intra-focal exposure and the other image from an extra-focal exposure. The intra- and extra-focal images are always from the same sensor, but different exposures.

The procedure is even simpler for the simulated images. The images are already paired up, and there is no background removal needed.

Another note we need to make here is the orthogonality issue we mentioned already in Section 1. In order to make a valid comparison, both algorithms need to use the same number of Zernike coefficients when estimating or fitting the wavefront. In the LSST algorithm configuration file, an option is provided to the user to use standard Zernikes, regardless of the obscuration of the system. However, we find that the agreements between the LSST and DECam algorithms are generally improved if we still use annular Zernikes in the LSST algorithm, then post-process the results by reconstructing a wavefront map from the annular Zernike coefficients then decomposing it into standard Zernikes. This is consistent with the fact that mathematically the TIE solvers in the LSST algorithm relies more on the orthogonality of the basis set. We use this post-processor to get the LSST results used in this comparison.

For the results shown in the next section, the LSST results are obtained using the series expansion algorithm as the baseline. As we discussed in Ref. 3, the two baseline algorithms produce very similar results. The series expansion algorithm is faster.

## 4. RESULTS

### 4.1 Comparison Using DECam Wavefront Sensor Data

Figure 2 shows the comparison of Zernike coefficients using one exposure from the open-loop wavefront images. Each plot is for one pair of wavefront sensors. For each wavefront sensor pair, the thin red dashed lines are the Zernike coefficients measured by the LSST algorithm for individual image pairs. The thick red solid lines are the average of all the LSST measurements. The thin blue (green) dashed lines are the DECam solutions without (with) quadrafoil for individual donut images. The thick blue (green) solid lines are the DECam averages without (with) quadrafoil. In general, the agreement on the averaged solutions between the algorithms is very

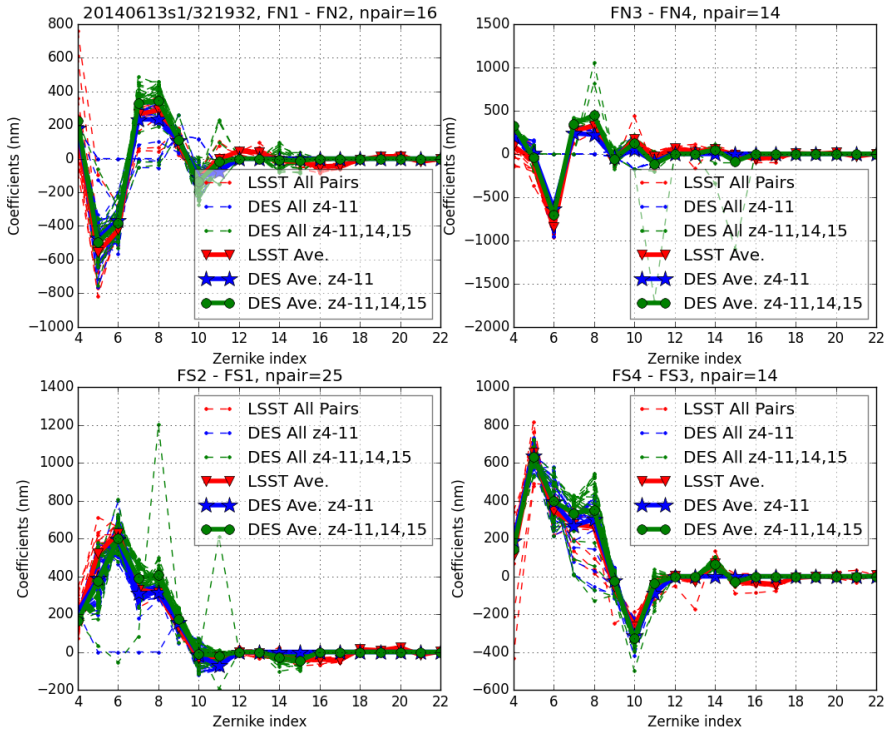


Figure 2. Comparison of Zernike coefficients using one exposure from the open-loop wavefront images.

good. Looking at the results from individual images, or image pairs in case of the LSST solutions, both algorithms are robust and give consistent results.

The comparison by Zernike between the two algorithms is shown in Figure 3. The DECam results are from the fits without quadrafoil. Very good agreement is seen for astigmatism, coma, and trefoil. Some deviations are seen on the focus term. Meanwhile the spherical aberration (Z11) coming out of the DECam algorithm has a very small spread. Apparently there is cross-talk between the focus and spherical terms in one or both algorithms. Focus and spherical aberration are both rotationally symmetric, and includes radial terms up to $\rho^2$ and $\rho^4$, respectively, where $\rho$ is the radial coordinate on the pupil. The difficulty in separating spherical from focus arises because of the limited number of pixels along the radial direction coupled with noise. The fact that the wavefront is different on adjacent wavefront CCDs also contributes to the differences between the results.

Results we have discussed so far are with the telescope in the open-loop mode. Next we will show some results from running both algorithms on wavefront sensor images during typical DECam observing runs. The scatter plots look similar to those in Figure 3, except that the aberrations are smaller and the range of variation of the aberrations are smaller. We have also looked at how the wavefront aberrations measured on the four pairs of wavefront sensors vary as a function of time throughout a typical DECam observing night. Figure 4 shows the time history of 45° astigmatism (Z5), as measured by both algorithms. Figure 5 is the coma-y (Z7) time history for the same night. The DECam wavefront is very stable over time. Generally good agreement is observed between the two wavefront sensing algorithms, in terms of both the absolute magnitude and the exposure-to-exposure variations. The RMS difference between the measurements made by the two algorithms is approximately in the range of 40 – 70 nm. This is true for all the other measured Zernikes. A missing data point on these plots means for a paticular exposure there is no pair of stars that could pass our saturation and SNR selections, which we described in Section 3.

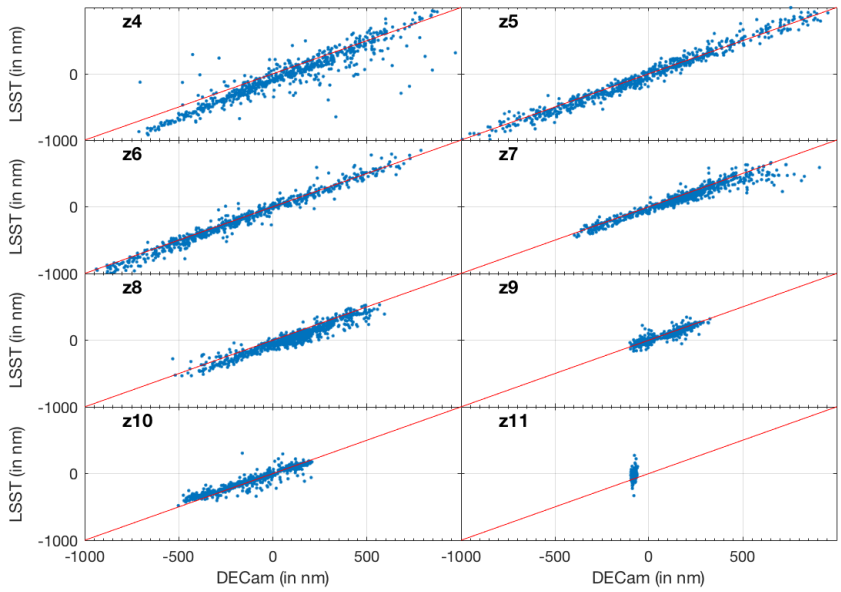


Figure 3. Scatter plots of DECam results vs. LSST by Zernike. The data used are wavefront sensor images with the telescope in open-loop mode. The red diagonal lines with slope of unit are for reference.

### 4.2 Comparison Using DECam Defocused Focal Plane Data

Comparison is also made using out-of-focus focal plane images taken during the engineering runs. These are also without the AOS corrections. As the result, the wavefront aberrations can also be a bit far from zero. Figure 6 shows the scatter plots comparing the two algorithms, for each Zernike separately. Looking at the Z4 plot in Figure 6, all image pairs show large focus term in the wavefront. In turn, this may have negatively impacted performance of the wavefront sensing algorithms. The LSST algorithm relies on the the intra- and extra-focal image planes stay well within the geometric limit.[3] It has long been observed that a large non-zero focus term affects the TIE-based algorithm's ability to recover the other wavefront Zernikes. Coma is a term easily affected, because it doesn't alter the boundary of the intensity distribution on the image. As the result, the TIE-based algorithm breaks down at relatively low magnitude of coma. Figure 6 shows good agreement between the two algorithms, except focus and coma. Other factors that might contributed to the differences between the results from the two algorithms include the temporal and spatial separations between the intra- and extra-focal images. Because the out-of-focus sensor images were taken at about 30 minutes apart, the underlying wavefront may have drifted to some degree. If the wavefront variation within a CCD chip is large, forming image pairs solely based on SNR without taking into account the location on the CCD may also introduce bias.

Figures 4 and 5 in Ref. 7 show how the DECam wavefront vary with coordinates on the focal plane. It is seen that the wavefront variation within single CCD chips is more pronounced at the edge of the focal plane. Therefore, if the agreement between the two algorithms can be improved by excluding the sensors on the outside of the focal plane in the above analysis, that would be evidence that the wavefront variation within chips is the major contributor to the differences in the results. However, the level of agreement between the two algorithms barely changes after we exclude the sensors on the outside of the focal plane. We have also looked at the defocused focal plane images where the camera is moved by $\pm$3.0mm. If this leads to better agreement between the results, we would have proven that it is the geometric limit that is affecting the performance of the LSST algorithm. No significant difference is observed between the $\pm$1.5mm and $\pm$3.0mm results. The exact source of the difference between results by the two algorithms, specifically on coma as shown in Figure 6, is currently unknown.

Another note to make here is the difference between pistoning the entire camera and the focal plane only. The LSST algorithm requires that the only change between the intra- and extra-focal images is the position of the focal plane. Moving the entire camera out of focus means the lenses are also moved. In principle, this

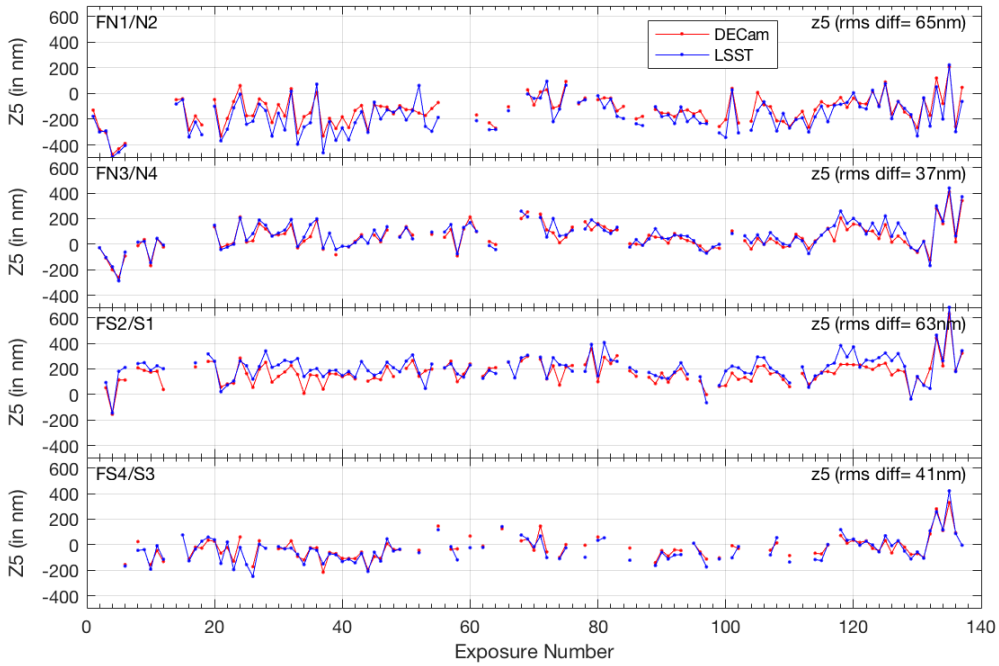


Figure 4. Variations of 45° astigmatism (Z5) through a typical DECam observing night, as measured by the DECam (red) and LSST (blue) algorithms. The four panels are for the four pairs of wavefront sensors. The RMS differences between the measurements by the two algorithms are shown in the upper right corner of each panel.

violates the requirements of the TIE solver. In practice, due to the low correcting power of the DECam corrector, which does little more than changing the $f$-number of the converging beam, the TIE still can be used, with a "effective" image offset. This is confirmed by creating intra- and extra-focal images with a ZEMAX DECam model by moving the focal plane and the entire camera separately, then running the images through the LSST algorithm. For DECam, the effective image offset is 1.2 times the real camera offset.

### 4.3 Comparison Using Simulated Data

Tests using simulated data is more straightforward, because they are not subject to the real-world effects like those discussed above. However, the simulated data suffer from certain artifacts, such as the approximations made in propagating the light and the effects of the atmosphere.

Figure 7 shows the comparison between the two algorithms using the donut images simulated by the DECam forward-modeling code. Note that in this test the DECam algorithm has the advantage of having the same optical model in both the simulated data and its forward fits. As we discussed in Section 2, the image pairs all have single-Zernike aberrations, with various magnitudes. The tests are done for Z4 – Z15. The missing DECam measurements are because the fit results didn't satisfy RMS(Z5–Z10)<3$\mu$m and 20$\mu$m< |Z4| <40$\mu$m.

Both algorithms perform well on astigmatism, trefoil, and quadrafoil.

For focus and spherical aberration, the comparisons between the input wavefront and measurements by both algorithms do not look good. The true input wavefront to the simulations are single-term circular Zernikes, while the LSST algorithm uses a finite number of annular Zernikes to recover the wavefront. Taking this into account, the difference in the two sets of results on focus and spherical doesn't necessarily mean that there is more significant cross-talk between focus and spherical aberration in the LSST algorithm. The DECam algorithm diverges when the spherical aberration gets larger than about 0.5$\lambda$, where $\lambda$=700nm. The DECam algorithm also fails with large second astigmatism (Z12, 13). Take note that Z11 is not a free parameter in DECam online operations, and Z12 and Z13 are not free parameters in DECam online or offline fits. Due to the geometric limit, the LSST algorithm's ability to recover coma starts to break down at around 1$\lambda$, where $\lambda$=700nm.

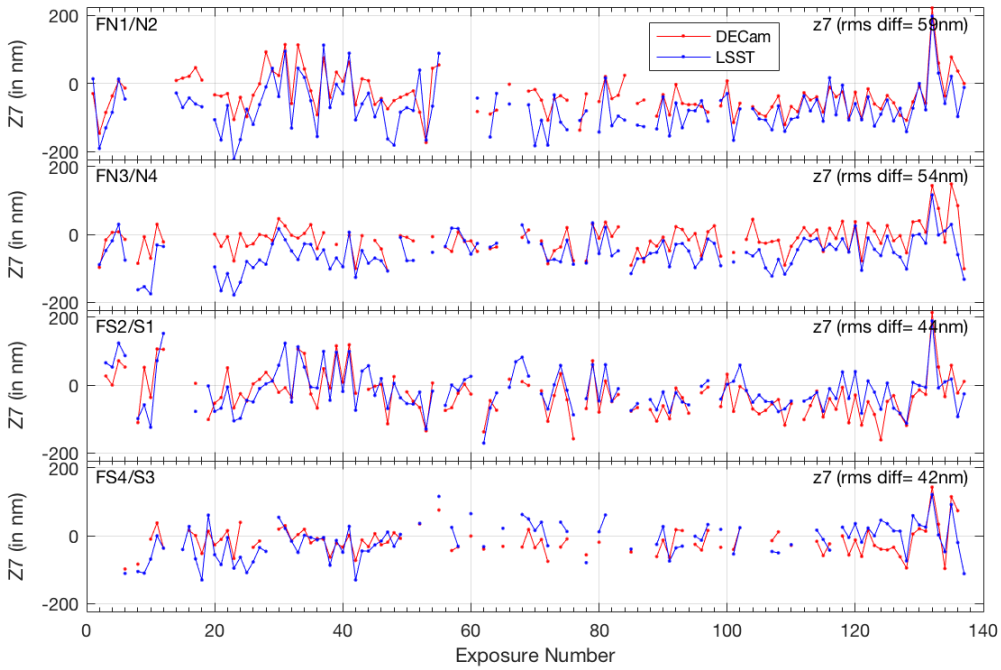


Figure 5. Variations of coma-y (Z7) through a typical DECam observing night, as measured by the DECam (red) and LSST (blue) algorithms. The four panels are for the four pairs of wavefront sensors. The RMS differences between the measurements by the two algorithms are shown in the upper right corner of each panel.

The same kind of comparison using the images simulated with the LSST-like paraxial ZEMAX model is shown in Figure 8. The ZEMAX model is independent of the LSST algorithm. For LSST results, some data points are missing due to a warning-flag that we are close to or outside of the geometric limit. Again, good agreement between the two algorithms is seen. For coma and spherical aberration, the LSST algorithm runs into geometric limit at around 700 – 800nm.

## 5. SUMMARY AND CONCLUSIONS

We have demonstrated good agreement between the TIE-based wavefront sensing algorithm used by LSST and the forward-modeling algorithm by DECam. The data used in this analysis include DECam images from both the wavefront sensors and out-of-focus focal plane and simulated images. The correction algorithms developed by LSST targeting fast $f$-number and wide-field systems are not tested here.

There appears to be some cross-talk between focus and spherical terms in one or both algorithms. Additionally, the LSST algorithm breaks down when certain aberrations, such as coma and spherical aberration, get large due to the geometric limit. However, a $\pm$1.5mm image offset for a $f/2.9$ system is equivalent to a $\pm$0.6mm offset for a $f/1.23$ system. The nominal wavefront sensor image offset for LSST is $\pm$2mm. With 10$\mu$m pixels, the LSST donuts will be about 165 pixels in diameter. We expect the geometric limit not an problem for LSST operation. The better pupil sampling and the use of the annular Zernikes on the annular pupil will both help reduce the cross-talk between Zernike modes with same azimuthal frequency.

Lastly, as we have seen on DECam, during normal observing, the wavefront aberrations measured by the wavefront sensors are small. For LSST, at the beginning of each night, the aberrations may be relatively large. As long as the wavefront retrieval algorithm doesn't break down, we expect the AOS will quickly pull the system back into convergence, so that it doesn't need to work anywhere close to the geometric limit.

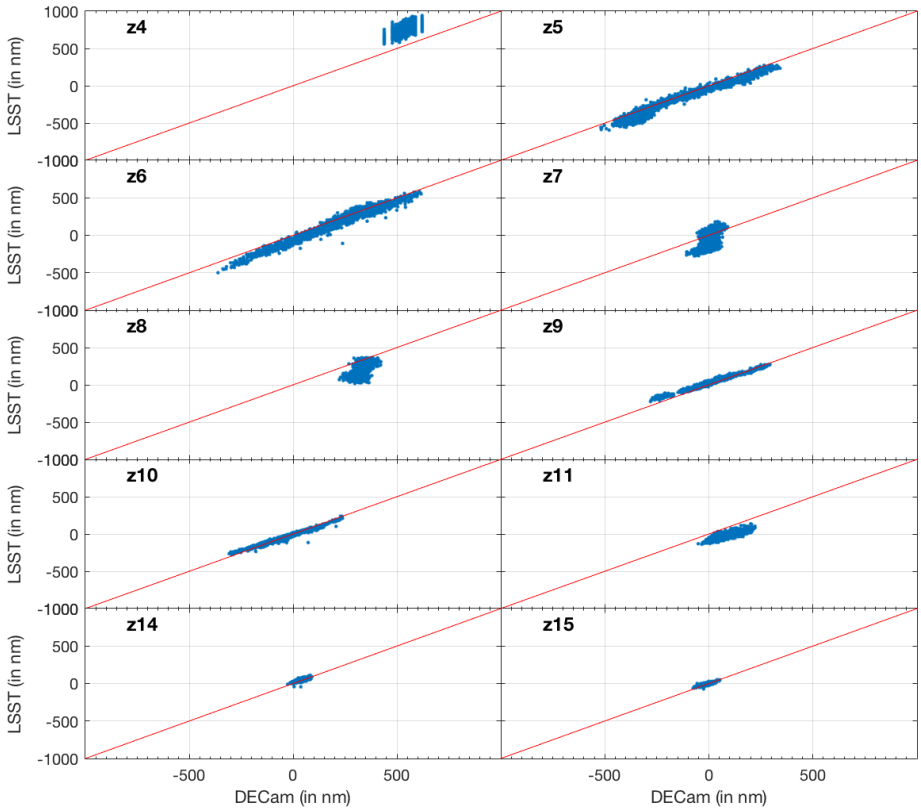


Figure 6. Scatter plots of DECam results vs. LSST by Zernike. The data used are out-of-focus science sensor data with the camera hexapod pistoned by ±1.5mm. The red diagonal lines with slope of unit are for reference.

## ACKNOWLEDGMENTS

We thank Paul Schechter for his critical comments on our work and helpful discussions. We also thank the LSST internal reviewer, Kevin Reil, for helping us improve the paper.

This material is based upon work supported in part by the National Science Foundation through Cooperative Support Agreement (CSA) Award No. AST-1227061 under Governing Cooperative Agreement 1258333 managed by the Association of Universities for Research in Astronomy (AURA), and the Department of Energy under Contract No. DEAC02-76SF00515 with the SLAC National Accelerator Laboratory. Additional LSST funding comes from private donations, grants to universities, and in-kind support from LSSTC Institutional Members.

## REFERENCES

[1] Kahn, S., "Final design of the large synoptic survey telescope," in [*Ground-Based and Airborne Telescopes IV*], *Proc. SPIE* **9906**, in press (2016).

[2] Ivezić, Ž. *et al.*, "LSST: from Science Drivers to Reference Design and Anticipated Data Products," *arXiv:0805.2366* **v4** (2008).

[3] Xin, B., Claver, C., Liang, M., Chandrasekharan, S., Angeli, G., and Shipsey, I., "Curvature wavefront sensing for the large synoptic survey telescope," *Applied Optics* **54**, 9045–9054 (2015).

[4] Roddier, C. and Roddier, F., "Wave-front reconstruction from defocused images and the testing of ground-based optical telescopes," *J. Opt. Soc. Am. A* **10**, 2277–2287 (1993).

[5] Guruyev, T. and Nugent, K., "Phase retrieval with the transport-of-intensity equation. ii. orthogonal series solution for nonuniform illumination," *J. Opt. Soc. Am. A* **13**, 1670–1682 (1996).

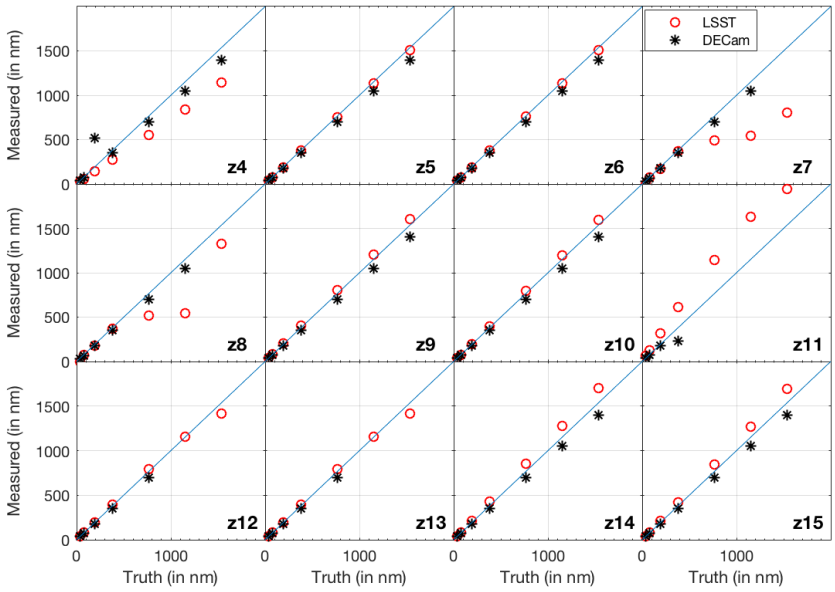


Figure 7. Comparison of wavefront recovery results using images simulated with the DECam forward-modeling code. The blue diagonal lines with slope of unit are for reference.

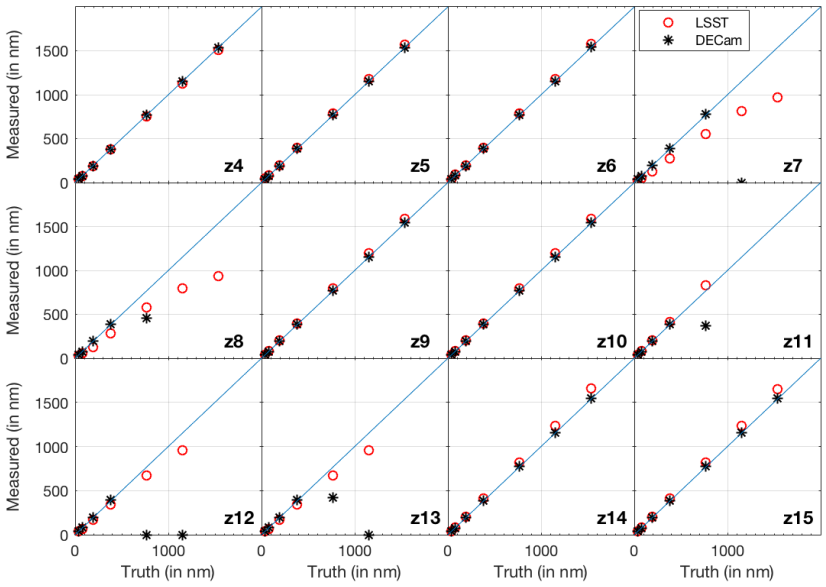


Figure 8. Comparions of wavefront recovery results using ZEMAX-simulated images. The blue diagonal lines with slope of unit are for reference.

[6] Flaugher, B. L. *et al.*, "Status of the dark energy survey camera (decam) project," in [*Ground-Based and Airborne Telescopes IV*], *Proc. SPIE* **844611**, 1–15 (2012).

[7] Roodman, A., Reil, K., and Davis, C., "Wavefront Sensing and the Active Optics System of the Dark Energy Camera," *Proc. SPIE* **9145**, 914516 (2014).

[8] Noll, R., "Zernike polynomials and atmospheric turbulence," *J. Opt. Soc. Am.* **66**, 207–211 (1976).

[9] Mahajan, V. N., "Zernike annular polynomials for imaging systems with annular pupils," *J. Opt. Soc. Am.* **71**, 75–85 (1981).